

ENCYCLOPEDIA OF LIFE SUPPORT SYSTEMS (UNESCO-EOLSS)

Chapter 6.3.2.4

WAVE MODELING AT THE SERVICE OF SECURITY IN MARINE ENVIRONMENT

Eva Bauer, Potsdam Institute for Climate Impact Research (PIK), Potsdam, Germany

Keywords

Wind-generated waves, Navier-Stokes equation, potential theory, Hamilton's principle, ray theory, wave action, energy spectrum, nonlinear interactions, wave generation, wave breaking, remote sensing, data assimilation, wave climate.

Contents list

1. Introduction
 - 1.1 Classification of waves
 - 1.2 History of wave modeling
 - 1.3 Outline of the article
2. Physical principles of free surface waves
 - 2.1 Statistical and spectral characteristics
 - 2.2 Wave kinematics in the domain of potential theory
 - 2.3 Wave kinematics in the domain of ray theory
3. Forcing functions for wave modeling
 - 3.1 Weak nonlinear wave-wave interactions S_{nl}
 - 3.2 Wave generation S_{in}
 - 3.3 Wave dissipation S_{ds}
4. Present applications of wave modeling
 - 4.1 Validation using global data
 - 4.2 Synoptic-scale wave predictions
 - 4.3 Coupled wind and wave data assimilation
5. Outlook

Glossary

angular wave frequency ω	Wave frequency f multiplied with 2π : $\omega = 2\pi f$ (rad s ⁻¹).
dispersion relation	Mathematical-physical relation between angular wave frequency ω and wave number k : $\omega = \omega(k)$, leading to the distinction between dispersive and non-dispersive waves. Dispersive waves may either show normal dispersion, with phase speeds increasing with wave number, or abnormal dispersion, with phase speeds decreasing with wave number.
fetch	Length scale on the sea surface along which the wind blows. Fetch for offshore winds corresponds to the distance from shore. A finite fetch (analogous to a finite wind duration) limits the wave growth, while infinite fetch (analogous to infinite wind duration) results in a fully developed wave field.
finite-amplitude wave	Wave with amplitude larger than that of a small-amplitude wave, having a non-sinusoidal wave form. Finite-amplitude waves are preferable subject to wave breaking.
long wave	Wave with a wavelength much longer than the water depth D , usually $L > 20D$, also called shallow water wave. Long waves are non-dispersive, i.e., their propagation speed is independent of the wave number.
peak frequency f_p	Frequency of the wave with the largest amplitude in a wave spectrum.
phase speed c_p	Wave speed given by the ratio of wavelength and wave period or the ratio of angular frequency and wave number: $c_p = LT^{-1} = 2\pi f k^{-1}$ (m s ⁻¹).
short wave	Wave with a wavelength shorter than twice the water depth D , i.e., $L < 2D$, also called deep water wave. Short waves are dispersive.
significant wave height H_s	Effective wave height which is proportional to the square-root of the total wave energy. Significant wave height, often reported by experienced observers, corresponds to the mean over the upper third of the surface elevations in a Gaussian distributed wave field (H_s in m).
small-amplitude wave	Wave of a small steepness, i.e. the amplitude a is much smaller than the wavelength: $aL^{-1} \ll 1$. Small-amplitude waves in deep water obey the first-order linear wave theory and have sinusoidal wave forms.
swell	Wind-generated waves which emanate from their generation region and propagate freely along the surface without influence from the winds blowing along their path. In deep water, swell waves represent short gravity waves which exhibit long crests.

SWAN	Third generation spectral wave model for shallow water.
WAM	Third generation spectral wave model.
wave amplitude a	Vertical surface elevation above equilibrium level corresponding to the radius of orbital motion of a sinusoidal wave (a in m).
wave frequency f	Inverse of the wave period: $f = T^{-1}$ (Hz).
wave height H	Vertical elevation of the crest above the trough (H in m). In case of a sinusoidal wave, the wave height corresponds to twice the amplitude a of that wave.
wavelength L	Horizontal distance between two wave crests measured at an instant of time (L in m).
wave number k	Inverse of the wavelength multiplied with 2π : $k = 2\pi L^{-1}$ (rad m^{-1}). In a two-dimensional field the wave number is a vector with two components.
wave period T	Time interval between two wave crests passing a fixed location (T in s).
wave spectrum	A wave spectrum can be obtained by the Fourier transformation of a time series of surface elevations, and describes the partitioning of the variance as a function of frequency. The integral over frequency of a one-dimensional frequency density spectrum, also called power density spectrum, is proportional to the total energy. A two-dimensional distribution of the variance as a function of frequency and direction or of the two-dimensional wave number vector represents a two-dimensional power density spectrum. Physical unit of a spectrum depends on the normalization. Commonly a one-dimensional spectrum is in $m^2 \text{ Hz}^{-1}$.
wave steepness	Ratio of wave height H and wavelength L , also known as the wave slope.
wind sea	Waves generated by wind forcing. The stronger the wind, and the longer the duration and the fetch of the wind forcing the larger the wave heights, their lengths and periods. In a region of wave generation, waves have different heights, lengths, periods and directions; thus wind sea exhibits short crests.
WKB approximation	Wentzel - Kramer - Brillouin approximation, which is applicable to waves in an inhomogeneous medium with slow variations of the inhomogeneities, and which is also known as the geometrical optics approximation.

Summary

Wind-generated waves are ubiquitous on the ocean surface. Blowing winds excite oscillations of the water surface with length scales ranging from millimeters to about a kilometer and time scales from less than a second to tenths of a minute. The associated wave amplitudes vary from less than a centimeter to several meters and the high waves may affect the safety of humans at sea. The wish to protect humans and to prevent damage to ships and constructions, expedited the development of numerical wave models in the second half of the 20th century. Theoretical investigations of wave generation, nonlinear wave-wave interactions and wave dissipation in conjunction with experimental investigations led so far to three generations of ocean wave models. Today, third generation wave models are established world-wide. Numerical wave modeling is used in various areas, such as engineering, ship-routing, and real-time wave prediction in connection with storm surge warning services. The growing interest in reliable real-time wave predictions calls for the development of a combined weather data and wave data assimilation scheme. Recent research corroborates the important role surface waves play in exchanging momentum, energy, gas and aerosols between the ocean and the atmosphere. Thus, in view of global climate changes, impact studies on potential wave climate changes and on potential changes in the marine ecosystem has opened a new area for wave modeling.

1 Introduction

1.1 Classification of Waves

Water waves represent a time-space varying phenomenon that obeys laws of geophysical fluid dynamics. Water waves are periodic motions of a density interface, and they propagate along the interface. These oscillations, either at the air-sea interface or at internal density interfaces below the sea surface, are transverse to the propagation direction. This implies upward and downward motions of the interface about its equilibrium level, since the dominant restoring force of an elevated interface is the force of gravity. Note that this is different for sound waves, which oscillate in the longitudinal direction in alignment with the propagation direction.

Wind-driven waves at the sea surface are of major importance for humans at sea and at the seaside. The wind-driven surface waves represent small to medium scale waves. The periods of wind-driven surface waves vary between a fraction of a second and 30 s, their wavelengths vary between centimeters and 1000 m, and their heights (from trough to crest) vary between millimeters and 30 m. A single extreme wave height within a group of waves is known as a rogue or freak wave. Freak waves evolve momentarily in stormy weather and are extremely dangerous to ships.

The shortest water waves on the interface between water and air are the capillary waves. Capillary waves, which are restored by surface tension of water, have periods of less than one tenth of a second and wavelengths of about one centimeter. They play a role in surface wave generation from an initial flat surface. Capillary waves coexist and interact with surface gravity waves. Knowledge of their properties is important for active microwave sensing, as microwave radars record signals backscattered by short waves with wavelengths of centimeters.

Examples of large-scale water waves are Tsunami, tides, Kelvin waves and Rossby waves. Tsunami are generated by underwater seismic activity and have periods in the range of 10 to 60 minutes. Tides are induced by gravitational forces of the Moon and the Sun exerted on the mass of the Earth. The dominant tidal periods are half-day and one-day long. Kelvin waves and planetary Rossby waves experience the effect of the Earth rotation (i.e., the Coriolis force) and are affected by lateral and bottom boundaries of the ocean basins. Interactions of the large-scale waves with the wind-driven waves can be neglected in usual conditions.

1.2 History of Wave Modeling

Wind-driven waves are ubiquitous on the ocean surface. The variable wind forcing, varying between weak winds and severe storms, induces surface waves of different amplitudes, periods, wavelengths and propagation directions. The thereby generated groups of waves transport energy along their propagation paths, and if propagation is linear, their mass transport is nil. When waves reach coastal zones, the wave energy is transformed and dissipated by various processes. Since in extreme wave situations the safety of humans at sea and onshore can be

severely threatened, the forecast of wave conditions had always been of concern.

The wish to forecast wave properties with wave models grew rapidly during the Second World War. Initially, a simple wave nomogram was developed to aid the planing of ship landings. Then, more sophisticated theoretical studies, and systematic laboratory and field measurements were conducted. Hence, numerical modeling of wind-driven waves developed progressively by reconciling theoretical knowledge with observational evidence. These efforts produced three generations of wave models. The distinction into three generations is connected with the treatment of the resonant nonlinear wave-wave interactions. These nonlinear interactions are the essential mechanism during wave growth, through which the peak frequency migrates to lower frequencies. The first generation models did not account for the nonlinear interactions, while the second generation models used a simplified parameterization of the nonlinear interactions. Then in third generation models, which are formulated for two-dimensional wave spectra, the nonlinear wave-wave interactions are explicitly computed.

Among the large number of measuring campaigns only the three most outstanding experiments in the field are briefly discussed here. The first experiment is the swell attenuation study in the Pacific presented by Snodgrass and others in 1966. The propagation of swell waves was traced over several thousands of kilometer. During their free propagation, the swell waves showed remarkable little attenuation. The second experiment, the Joint North Sea Project (JONSWAP), was conducted to measure the evolution of a wave spectrum in dependence of the wind vector, the fetch and other relevant parameters. The results, summarized by Hasselmann and others in 1973, yielded a parametric form of the frequency spectrum of wind-driven waves (JONSWAP spectrum) and empirical growth curves for the nondimensional wave energy and the nondimensional wave peak frequency. The nondimensionalization is obtained using elementary quantities, namely the wind stress forcing and the acceleration of gravity. The growth curves describe the exponential rates of the growth of nondimensional wave energy, and of the decrease of nondimensional peak frequency, both for growing fetch and growing duration of wind forcing. After sufficient long time of wind forcing, the speed of the dominant wave approaches the wind speed (taking a few hours for small fetches and small wind speeds until several days for long fetches and strong wind conditions). Then, the transfer of energy from the atmosphere eases off, and the wave growth reaches saturation. The third experiment, carried out in the Bight of Abaco and presented by Snyder and others in 1981, provided an empirical base for an appropriate wind input function in third generation wave models.

Today, third generation wave models are applied in different fields, such as for real-time predictions of global and regional wave fields, for engineering purposes, for climate change studies, and for scientific research. The real-time predictions are useful for, e.g., the planing of optimal ship routes, and coastal warning services together with storm surge predictions. The interest of engineers is on the design of efficient ship structures, offshore constructions and coastal protection barriers, which can withstand the impact of waves. Analyses of long-term changes in the wave climate are essential for coastal protection measures. Aspects of scientific research are the refinement of the numerical modeling with respect to the manifold interaction processes at the interfaces between the water and the overlying air and the underlying bottom. Further

research is undertaken to improve data assimilation schemes. Data assimilation is needed to exploit the real-time data from satellite-based remote-sensing instruments which provide a wealth of information on global wind fields and ocean wave fields.

1.3 Outline of the Article

In an international collaborative effort, in which numerous groups were engaged to develop an advanced and efficient wave model, the third generation wave model WAM was created. In the following, a few key points concerning the theoretical base of a third generation wave model will be addressed. For a broader elaboration on wave modeling the reader is asked to consult the annotated bibliography and the references therein.

Section 2 addresses the physical principles of free ocean surface waves. The wave field can be seen as an ensemble of monochromatic waves which randomly disturb the mean sea level. Useful definitions to describe the properties of a monochromatic wave, as well as the statistical properties of a field of waves are listed in the Glossary. Distributions of wave heights are usually described by either their probability distribution or their spectral power distribution (section 2.1).

The mathematical-physical description of the kinematics and the dynamics of surface waves is based on two different approaches. The first approach uses the Navier-Stokes equation which is known in classical oceanography as the equation of motion in a viscous medium. This approach leads to the Laplace equation for waves in the domain of potential theory. The first-order solution of the Laplace equation, which is valid for small-amplitude waves, yields the dispersion relation for homogeneous media, elucidating the behavior of linear plane waves (section 2.2).

The second approach of the mathematical-physical description employs Hamilton's principle of classical mechanics. The Hamilton principle is applied to an ensemble of linear waves which constitutes a wave group. The evolution of the properties of a wave group is then formulated in analogy to quantum mechanics for inhomogeneous media. In doing so, the ocean wave field is decomposed into different wave groups characterized by their wave numbers and their spectral action densities. The wave action density is the adiabatic invariant in an inhomogeneous system. Here, the inhomogeneous system is the ocean and the inhomogeneity is caused by varying ocean depth and currents. From the variational principle follows the radiative transfer equation of the spectral wave action density, which is also known as the transport equation of wave action in the domain of ray theory. In a homogeneous and time-invariant ocean the transport equation of the spectral action density reduces to the transport equation of the spectral energy density (section 2.3).

Usually, numerical wave models, describing the kinematics and dynamics of surface waves, are based on the radiative transport equation. One of the reasons is that the resonant nonlinear wave-wave interactions can be reconciled with the radiative transfer equation. The nonlinear interactions enter the transport equation as a forcing function in addition to the functions of wave generation and wave dissipation (section 3). The nonlinear interactions are derived from

theoretical considerations. They involve neither gain nor loss of the wave action, but a redistribution of wave action density among four resonant wave groups (section 3.1). Wave generation is induced by the transfer of energy from the atmospheric flow to the sea surface (section 3.2). Wave dissipation results from wave breaking at the surface and from friction at the sea floor (section 3.3). The source functions of wave generation and dissipation are also theoretically founded, but require adjustment to empirical evidence.

Section 4 presents global applications of the third generation model WAM. The quality of global WAM predictions could be tested for the first time after polar orbiting satellites started to measure wave data by remote-sensing techniques. The agreement between monthly means of modeled and remote-sensed wave height data is reasonably good (section 4.1). Real-time wave predictions, which are obtained by driving the wave model with actual wind fields from a synoptic weather model, are nowadays widely established. The synoptic wind forcing induces synoptic-scale variability in the wave data which frequently contain large deviations from the corresponding monthly mean (section 4.2). Nowadays, wave forecasts a few days ahead are routinely carried out using assimilation methods involving coupled wave-atmosphere models (section 4.3).

The closing section 5 gives a brief outlook on present wave modeling activities in the global and the regional perspective and in view of global climate change.

2 Physical Principles of Free Surface Waves

2.1 Statistical and Spectral Characteristics

Ocean surface waves appear as time-varying random elevations of the mean sea level. Such an appearance may arise from the superposition of many single sine waves with different periods, amplitudes and propagation directions. If the surface elevations are assumed to be locally homogeneous, stationary and Gaussian distributed, and the phases of the waves (i.e. the arguments of the sine functions) are evenly distributed, then the distribution of wave heights is completely described by the second statistical moment of an ensemble of randomly varying elevations. Based on the ergodic theorem, the second moment of an ensemble is equivalent to the variance of the elevation time series at a location.

The total energy E_{tot} per unit area of free sine waves is proportional to the variance of the surface elevations:

$$E_{tot} = \frac{1}{2} \rho g \langle \eta^2 \rangle \quad (1)$$

where $\langle \eta^2 \rangle$ is the variance of elevations η , ρ the density of water and g the gravitational acceleration. Instead of using the total energy an effective height scale, i.e., the significant wave

height H_s

$$H_s = 4\sqrt{\langle \eta^2 \rangle} \quad (2)$$

is commonly used. The significant wave height can alternatively be determined as the mean of the upper third of the height-sorted elevations. This follows from the Gaussian distribution of the elevations on the two-dimensional sea surface or from the narrow spectrum assumption. For the open ocean, the assumption of a Gaussian distribution is most of the time valid, as the space and time scales of generation and dissipation processes are usually much larger than the typical wavelengths and periods of the waves. Deviations from the Gaussian distribution and thus from linear wave theory occur in shoaling water with decreasing water depth, and especially in the surf zone. In the surf zone the waves become steep and nonlinear interactions induce wave breaking.

One advantage of the Gaussian assumption is that the statistical second moment of the surface elevations is directly related to the integral over all frequencies of the frequency spectrum

$$\langle \eta^2 \rangle = \int_0^\infty E(f) df \quad (3)$$

where $E(f)$ is the spectral power density depending on frequency f . The spectral power density can be obtained according to the Wiener-Khinchine theorem by the Fourier transformation of the autocorrelation function of the elevation time series. The same transformation is applicable to a two-dimensional random wave field where the waves propagate in the horizontal plane. The spectral power density per unit area is then described by the two-dimensional wave number spectrum which can be equivalently expressed by the frequency-direction spectrum (see section 4.2).

2.2 Wave Kinematics in the Domain of Potential Theory

The basic equation of oceanic motions is the Navier-Stokes equation. For free surface waves, the Navier-Stokes equation reduces to the two-dimensional Laplace equation. The Laplace equation characterizes a potential field of irrotational and source-free flow. The reduction is a consequence of the following approximations:

- The frequency of wind-generated surface waves is three to four orders of magnitude smaller than the frequency of Earth rotation and consequently the effect of the Coriolis force is negligible.
- The Reynolds number for surface waves is large which implies that inertial forces are much larger than viscous forces, and the water may be considered inviscid. (The Reynolds number

is defined as $Re = cL\nu^{-1}$ where c is a typical speed, L a length scale, and ν the kinematic viscosity of water. Setting $c = 1 \text{ ms}^{-1}$, $L = 1 \text{ m}$ and $\nu \approx 10^{-6} \text{ m}^2 \text{ s}^{-1}$ results in $Re \approx 10^6$.)

- For wavelengths longer than about 0.1 m the restoring force of gravity dominates the surface tension.
- The compressibility of water is negligible for surface waves.
- The conservation equation of mass for incompressible water implies a flow without divergence.

Solving the Laplace equation for water waves, and fulfilling the boundary conditions, involves a Taylor series expansion with respect to wave amplitude. The first-order solution, valid for a small-amplitude wave, leads to the linear wave equation. For linear waves, water parcels move in circles in the vertical plane completing an orbit in one wave period. The radius of the circle decreases exponentially with growing water depth (i.e., surface waves are truly a phenomenon of the upper ocean). In shallow water the path of the water parcel becomes elliptical and degenerates to a straight line parallel to the bottom. From this it is obvious that linear waves do not transport mass.

The frequency-wave number characteristic of first-order linear waves is given by the dispersion relation. The dispersion relation for capillary-gravity waves, where the restoring force is the combination of surface tension and gravity, reads:

$$\omega = \sqrt{(gk + Sk^3\rho^{-1}) \tanh(kD)} \quad (4)$$

where $\omega = 2\pi f$ is angular frequency, g acceleration of gravity, k wave number (for simplicity, only the modulus of the wave number vector is considered), D water depth, S surface tension of water ($S \approx 0.073 \text{ Nm}^{-1}$), and ρ density of water ($\rho \approx 10^3 \text{ kgm}^{-3}$). From the dispersion relation follows that the phase speed depends on wave number:

$$c_p = \omega k^{-1} = \sqrt{(gk^{-1} + Sk\rho^{-1}) \tanh(kD)} \quad (5)$$

In deep water, the wavelength is short relative to the water depth. So when $kD > \pi$ and $\tanh(kD)$ approaches 1, the phase speed of capillary-gravity waves is independent of water depth:

$$c_p^d = \sqrt{gk^{-1} + Sk\rho^{-1}} \quad (6)$$

Waves with wavelengths longer than 0.1 m are pure gravity waves, which means that the effect of surface tension is negligible. When short linear waves reach shallow water they become long

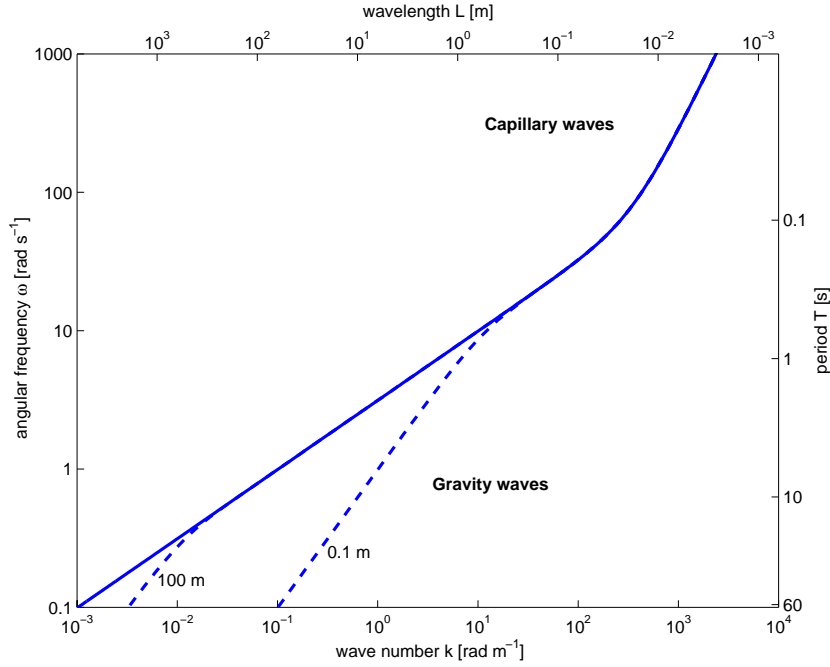


Figure 1: Dispersion relation between angular frequency ω (rad s^{-1}) and wave number k (rad m^{-1}) for surface capillary-gravity waves in deep water (continuous line) and for gravity waves in shallow water (dashed lines) of depth 0.1 m and 100 m.

waves. In shallow water, when $kD < 0.1\pi$ and $\tanh(kD)$ approaches kD , the phase speed of gravity waves reads:

$$c_p^s = \sqrt{gD} \tag{7}$$

Hence, the phase speed of waves propagating into shallow water decreases in proportion to the square-root of water depth. The decrease of the phase speed is associated with a proportional decrease in wavelength. This results from the law of conservation of the number of wave crests, which states that the number of wave crests passing a fixed location remains constant with time.

The dispersion relation for capillary-gravity waves is displayed in Figure 1. This diagram spans four orders of magnitude of wave frequency (or period) and seven orders of magnitude of wavelength (or wave number). This wide range of time and length scales is characteristic for wind-driven waves. The wave period grows with wavelength, but differently for different types of waves. In deep water, the period grows nonlinearly with wavelength, namely L is proportional to $T^{2/3}$ and T^2 for capillary and gravity waves, respectively. But in shallow water the period grows linearly with wavelength.

The energy of waves is transported by a group of waves with its group velocity. The group velocity is defined as the partial derivative of the dispersion relation with respect to the wave

number vector, where here for simplicity the modulus of the wave number vector is taken, yielding the group speed:

$$c_g = \frac{\partial \omega}{\partial k} \quad (8)$$

In deep water, the group speed of capillary-gravity waves is:

$$c_g^d = \frac{1}{2kc_p^d} (g + 3Sk^2\rho^{-1}) \quad (9)$$

and in shallow water the group speed of gravity waves equals the phase velocity:

$$c_g^s = \sqrt{gD} = c_p^s \quad (10)$$

Figure 2 shows the changes of the phase speed (equation 6) and the group speed (equation 9) with wavelength for capillary-gravity waves in deep water. The minimum phase speed is 0.23 ms^{-1} which occurs at wavelength $L_t = 0.017 \text{ m}$. The wavelength L_t marks the transition between normal dispersion, where the phase speed increases with wavelength (gravity waves), and abnormal dispersion, where the phase speed decreases with wavelength (capillary waves). At L_t , wave phase speed and group speed are equal. The influence of shallow water on the speeds of gravity waves is displayed, for instance, for the water depth $D = 0.1 \text{ m}$. In this shallow depth, the waves with wavelength L larger than 2 m are no more dispersive. Non-dispersive waves have phase speeds equal to their group speeds and both are independent of wave number.

In the open ocean, the linear wave theory is usually applicable, because waves have small amplitudes with wave steepness seldom larger than 0.08. Without claim of completeness, two simple analytical solutions for finite-amplitude waves are noted. First, the third-order solution of the Laplace equation leads to the Stokes wave. The Stokes wave has no vorticity but a horizontal drift current, called the Stokes drift. Second, an exact solution of the Navier-Stokes equation formulated in Lagrangian terms leads to the Gerstner wave. The form of the Gerstner wave is trochoidal. The Gerstner wave has no drift current but has vorticity and thus falls outside the domain of potential theory. In conditions when the wave steepness exceeds 0.08, the wave properties are more complex and wave motions contain portions of rotational flows and drift currents. So, with increasing wave steepness the suitability of the potential theory decays quickly.

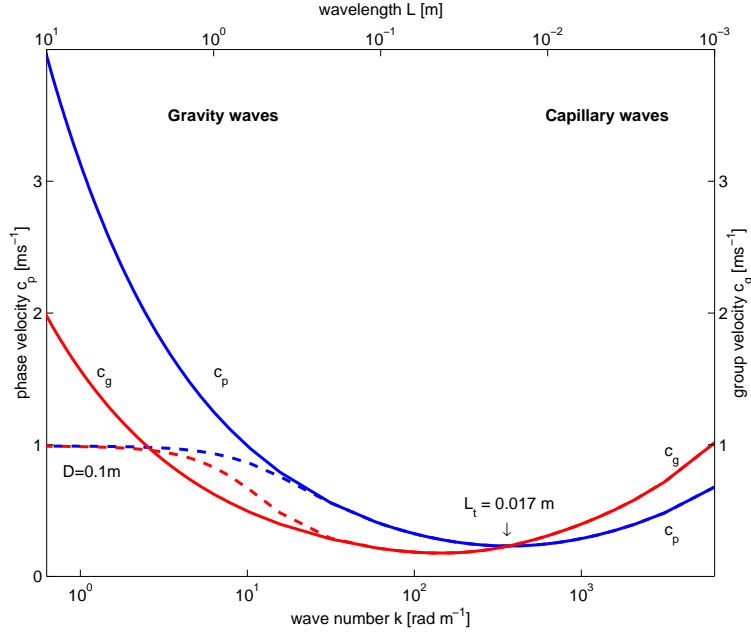


Figure 2: Phase speed c_p in ms^{-1} (blue line) and group speed c_g in ms^{-1} (red line) as function of wave number k (rad m^{-1}) or wavelength L (m) for gravity and capillary waves. Transition wavelength from normal dispersion (gravity waves) to abnormal dispersion (capillary waves) is $L_t = 0.017$ m. Continuous lines are for deep water waves. Dashed lines are for gravity waves in shallow water of 0.1 m depth which are non-dispersive for wavelengths larger than 2 m.

2.3 Wave Kinematics in the Domain of Ray Theory

Wave groups in an inhomogeneous medium transport wave action density. On the assumption that the WKB approximation is applicable, the transport can be described by the ray transport equation. The ray transport equation is defined in the four-dimensional phase space, which is spanned by the horizontal coordinates x and y and the horizontal wave numbers k_x and k_y . The rays are defined by the canonical Hamilton equations. Here, the horizontal coordinates $x_i, i = 1, 2$ are considered as the canonical coordinates, and the wave numbers $k_i, i = 1, 2$ as the canonical momenta. The Hamilton equations describe the time-changes of the coordinates, i.e., the group velocities, and of the wave numbers, i.e. the horizontal changes of the angular frequency:

$$\frac{dx_i}{dt} = \dot{x}_i = \frac{\partial \Omega}{\partial k_i} \quad (11)$$

$$\frac{dk_i}{dt} = \dot{k}_i = -\frac{\partial \Omega}{\partial x_i} \quad (12)$$

The angular frequency Ω is given by

$$\begin{aligned}
\Omega(x_i, k_i) &= \sqrt{gk \tanh(kD(x_i, t))} + k_i u_i(x_i, t) \\
&= \omega_0(x_i, t) + k_i u_i(x_i, t)
\end{aligned}
\tag{13}$$

where Ω is the so-called Hamiltonian which corresponds to the dispersion relation. The dispersion relation Ω is formulated for an inhomogeneous medium, in which the depth D and the current components u_i , $i = 1, 2$ may vary with the horizontal coordinates x_i and time t . In the second term of the right hand side of equation (13) the summation convention over the recurring index i is adopted which is used hereafter. The frequency ω_0 denotes the intrinsic frequency. In case of a homogeneous medium with constant water depth and no currents the dispersion relation reduces to

$$\omega_0 = \sqrt{gk \tanh(kD)}
\tag{14}$$

which corresponds to the dispersion relation (4) inferred above from linear wave theory for the small-amplitude gravity waves.

In the four-dimensional phase space, in which the properties of the medium vary little in time and space compared to the wave periods and wavelengths, the wave action density is an adiabatic invariant. This means, that the wave action N is conserved during the propagation of a wave group along its ray, provided the propagation is free, i.e., without generation and dissipation source functions. Hence the wave action transport equation in a field of slowly varying depth and current reads in the flux form:

$$\frac{d}{dt}N = \frac{\partial}{\partial t}N + \frac{\partial}{\partial x_i}(\dot{x}_i N) + \frac{\partial}{\partial k_i}(\dot{k}_i N) = 0
\tag{15}$$

The wave action propagating along rays is defined by the spectral wave energy $E(k_i; x_i, t)$ divided by the intrinsic frequency ω_0 :

$$N(k_i; x_i, t) = \frac{E(k_i; x_i, t)}{\omega_0}
\tag{16}$$

If the medium is homogeneous and with constant currents then the spectral wave action transport equation (15) reduces to the transport equation of the spectral wave energy E in the flux form:

$$\frac{d}{dt}E = \frac{\partial}{\partial t}E + \frac{\partial}{\partial x_i}(\dot{x}_i E) = 0 \quad (17)$$

where $\dot{x}_i = \partial\omega_0/\partial k + u_i$ with $i=1,2$ and $\partial\omega_0/\partial k$ is the wave group velocity.

The transport of wave action or wave energy along rays is called linear as the transport along one ray is independent from the transport along another ray. Accordingly the transport of the wave action is comparable with the propagation of the light in geometrical optics. In deep water without currents the propagation ray is a straight line which corresponds to a great circle on the spherical Earth. Deviations from the straight line occur when waves groups reach shallow water. In decreasing water depth, rays are refracted towards the direction of the normal (i.e. perpendicular) to the shoreline. Again this is in analogy to geometrical optics where light is refracted in a density-varying medium. In water with constructions, waves experience effects also from diffraction at obstacles, reflection at elongated structures, and wave breaking. The presence of sea ice induces scattering and damping effects of surface waves which depend strongly on the relative length scales of the ice flows and the waves.

Wave propagation is no longer free when waves are subject to a forcing function S_{tot} , i.e.,

$$\frac{d}{dt}E = S_{tot} = S_{nl} + S_{in} + S_{ds} \quad (18)$$

In the open ocean, the most important terms of the total source function S_{tot} of the energy transport equation are the resonant nonlinear interactions S_{nl} , the wind input source function S_{in} and the dissipation due to white capping S_{ds} .

3 Forcing Functions for Wave Modeling

3.1 Weak Nonlinear Wave-wave Interactions S_{nl}

The nonlinear wave-wave interactions of third-order are weak-in-the-mean because their effective time scale during wave growth is relatively large. Nonlinear interactions are active until saturation is reached which may take from hours to days, thus lasting longer than the typical period of surface waves. The nonlinear interactions are called third-order as they describe the evolution of a wave group which is in resonance with three other wave groups of the wave field. This four-wave interactions of third-order is the lowest order for gravity waves being resonantly coupled. The resonance conditions are:

$$\mathbf{k} = \mathbf{k}_1 + \mathbf{k}_2 - \mathbf{k}_3 \quad (19)$$

$$\omega = \omega_1 + \omega_2 - \omega_3 \quad (20)$$

where \mathbf{k}, \mathbf{k}_j with $j = 1, 2, 3$ are the two-dimensional wave number vectors and ω, ω_j the corresponding intrinsic wave frequencies.

The nonlinear interactions redistribute spectral wave action mainly from higher to lower frequencies, until when a fully developed spectrum is achieved. A fully developed spectrum has the shape of a skewed bell, with a cut-off at low wave numbers and a long, high wave number tail. The total wave action remains unchanged through the resonant nonlinear interactions:

$$\int N(\mathbf{k}) d\mathbf{k} = const \quad (21)$$

The nonlinear wave-wave interactions also conserve momentum

$$\int \mathbf{k}N(\mathbf{k}) d\mathbf{k} = const \quad (22)$$

and energy

$$\int \omega_0 N(\mathbf{k}) d\mathbf{k} = const \quad (23)$$

For the wave vector \mathbf{k} the rate of change of the spectral wave energy is obtained by solving the six-dimensional Boltzmann integral:

$$S_{nl}(\mathbf{k}) = \int G(\mathbf{k}_1, \mathbf{k}_2, \mathbf{k}_3, \mathbf{k}) R d\mathbf{k}_1 d\mathbf{k}_2 d\mathbf{k}_3 \quad (24)$$

where the factor R is

$$R = [N_1 N_2 (N_3 + N) - N_3 N (N_1 + N_2)] \delta(\mathbf{k}_1 + \mathbf{k}_2 - \mathbf{k}_3 - \mathbf{k}) \delta(\omega_1 + \omega_2 - \omega_3 - \omega) \quad (25)$$

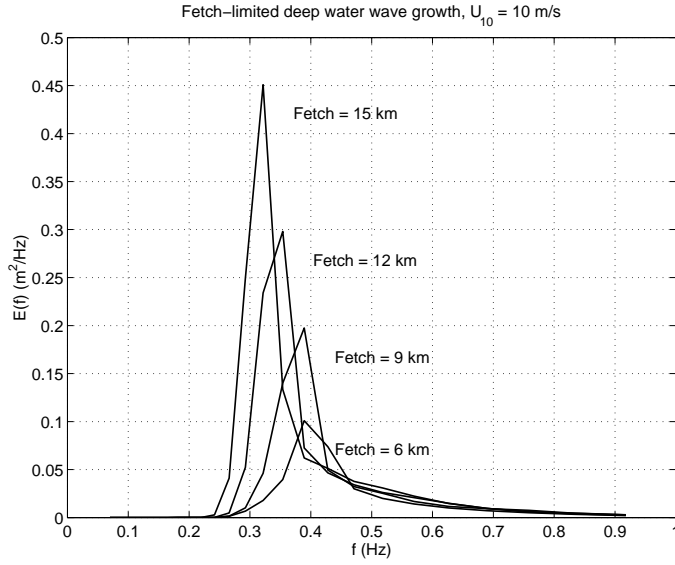


Figure 3: Fetch-limited frequency spectra $E(f)$ in m^2Hz^{-1} shown for growing fetch of 6, 9, 12 and 15 km in deep water with constant wind forcing of 10 ms^{-1} . The fetch-limited spectra are obtained after the waves reached saturation from a third generation wave model with the exact calculation of the nonlinear wave-wave interactions.

and $N_j(N)$ denotes the wave action density of the wave number vector $k_j(k)$. The two δ -functions represent the resonance conditions. The coupling coefficient G is a complicated function not further discussed here.

Solutions of the integral, which are non-trivial, show that changes of the wave action within the spectrum have a three-lobe structure. This structure displays the transfer of action at the expense of action from an intermediate wave number range to mostly lower wave numbers, although some action leaks to higher wave numbers. The behavior is also called “overshoot effect”. The overshoot effect exhibits the fact that the maximum spectral energy at the peak frequency in an early state of wave growth, before the wave field has fully developed, exceeds (overshoots) the spectral wave energy contained at this frequency in a succeeding state, whereby the peak frequency successively shifts to lower frequencies. The effect of nonlinear interactions on the evolution of a one-dimensional frequency spectrum with growing fetch is shown in Figure 3.

The basics of the nonlinear interactions were published in 1962 by Hasselmann, and in 1985 Hasselmann and others introduced an efficient computation method for the nonlinear transfer function S_{nl} . The computation of S_{nl} was simplified by employing symmetry properties of the Boltzmann integral which led to the discrete interaction approximation (DIA). Further adaptations of the integral were derived for shallow water waves. The assumption that nonlinear wave-wave interactions are weak-in-the-mean breaks down in situations of enhanced wave breaking. Moreover, in coastal zones with irregular bottom topography also the effects of the triad wave interactions gain importance.

3.2 Wave Generation S_{in}

Studies on the process of wave generation through wind forcing have a long history. In 1957 two independent theoretical mechanisms for energy transfer from the atmospheric boundary layer to surface waves were put forward. First, Phillips proposed a mechanism based on normal pressure fluctuations, which is consistent with the irrotational wave motion. This mechanism implies linear wave growth with time. However, linear wave growth is found to satisfy only the initial wave growth starting from a flat surface. Second, Miles formulated a resonance condition between the tangential shear flow in the boundary layer and the wave motion. This implies that the spectral generation function is directly proportional to the spectral wave energy $E(\mathbf{k})$

$$S_{in}(\mathbf{k}) = \beta\omega E(\mathbf{k}) \quad (26)$$

where \mathbf{k} is the wave number, ω the angular frequency, and β the nondimensional growth rate, which depends on the atmospheric wind profile. This mechanism produces an exponential wave growth with time which is compatible with observations of the advanced wave growth. However, the measurements in the Bight of Abaco (1981) showed only an order of magnitude agreement, indicating that the theory underpredicts the energy transfer rate. An appropriate parameterization of the input source function was then proposed:

$$S_{in}(\mathbf{k}) = \max\left[0, 0.25 \frac{\rho_a}{\rho} \left(\frac{u}{c_p} \cos \theta - 1\right) \omega E(\mathbf{k})\right] \quad (27)$$

where ρ_a, ρ are the densities of air and water, respectively, u is the wind speed, c_p the phase speed and θ the angle between the wind vector and the direction of wave propagation. This function forces waves of those wave numbers for which the aligned wind speed is larger than their phase speeds. For waves traveling faster than the wind no energy input occurs. Various extensions of the parameterization to account for the turbulence in the air flow and the feedback mechanism of the waves on the atmospheric flow resulted in relatively small improvements of the input function.

3.3 Wave Dissipation S_{ds}

The dissipation of the wave energy is induced by viscous dissipation (i.e., the generation of heat at the expense of the wave mechanical energy), wave breaking and bottom friction. Viscous dissipation occurs for very short gravity waves and capillary waves and is negligible for large-scale waves.

The processes involved in the wave breaking phenomena are not yet completely understood. Wave breaking on the sea surface is highly intermittent and localized. In the open ocean, breaking of waves is mostly connected with the white capping process. White caps are in geometric

similarity to the underlying wave: they are situated at the forward face of the wave and attenuate wave energy through turbulent interactions. Since field measurements of the pure mechanism of wave dissipation are not possible with active wind forcing, the dissipation source function is determined by indirect means. A commonly used approximate relation is obtained by assuming that the spectral dissipation function is proportional to the wave energy and the angular wave frequency

$$S_{ds}(\mathbf{k}) \propto -\omega E(\mathbf{k}) \quad (28)$$

An appropriate scaling of the white capping dissipation function for numerical modeling was determined in 1984 by Komen and others. This was achieved by adjusting the dissipation function such, that measurements of the spectral shape and the wave growth curves were reproduced by calculations with the wave transport equation.

In coastal zones, transformations of the wave energy lead to current modifications, turbulent mixing and sediment transport. The waves break when a characteristic, empirical quantity, which depends on wave height, wave period, wave slope and bottom slope, exceeds a threshold value. Depending on these properties, four types of breakers are distinguished, namely the spilling, the plunging, the collapsing and the surging breaker.

Bottom dissipation occurs for long waves, i.e., for $kD < 3$ where k is the wave number and D the water depth. The smaller the value of kD the stronger the interactions of the waves with the bottom. The interactions with the bottom are divided into the effects motion of a soft bottom, the percolation through a porous bottom and the friction in the turbulent bottom boundary layer. The bottom friction is commonly parameterized by the eddy-viscosity concept. Dissipation through interactions of deep water waves with tidal currents is generally found to be negligible.

4 Present Applications of Wave Modeling

4.1 Validation using Global Data

As described above numerical wave models were continuously validated against experimental evidence obtained either in laboratories or in the field, but a global validation, with global homogeneous measurements, had been impracticable until 1978. The first global validation of modeled significant wave heights using the wave model WAM was possible with measured H_s data obtained from the radar altimeter aboard the American satellite SEASAT, flown on a polar orbit. The altimeter H_s data are inferred from the time-varying shape of the microwave signal which is received from the sea surface by the nadir-viewing radar altimeter. The agreement between modeled and measured H_s data was remarkably close, but the analysis was time-limited because SEASAT operated only for a 3-month period in 1978. Thereafter the altimeter wave

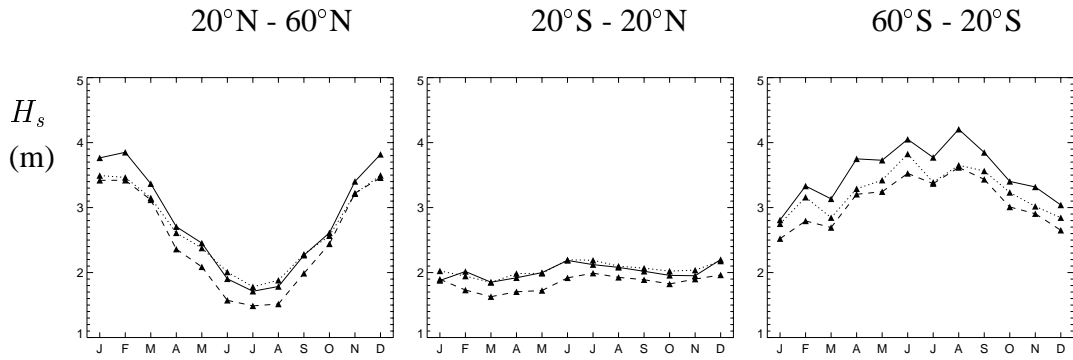


Figure 4: Monthly means of co-located H_s (m) obtained from the real-time predictions with the wave model WAM (dashed line), the radar altimeter aboard the TOPEX/POSEIDON satellite (continuous line) and the Synthetic Aperture Radar (SAR) aboard the ERS-1 satellite (dotted line) for 1994. Monthly means are displayed for the northern latitudes between 20°N and 60°N (left panel), the tropical latitudes between 20°S and 20°N (middle panel) and for the southern latitudes between 60°S and 20°S (right panel).

data from the American satellite GEOSAT operating from 1985 until 1990 enabled global multi-year comparisons.

From 1991 onward not only altimeter H_s data from the European Remote Sensing satellites (ERS-1 and ERS-2) and from the American-French satellite TOPEX-POSEIDON were available but also two-dimensional wave spectra measured by a Synthetic Aperture Radar (SAR) aboard ERS-1 and ERS-2. The SAR is a slant-viewing radar which receives microwave signals from the sea surface through the coherent Bragg scattering mechanism. The Bragg scattering mechanism, known from the field of crystallography, is based on a resonance condition between the wavelength of the incident electromagnetic wave and the regular spacing of the scattering targets. The scattering targets of the SAR microwaves are the elevations of the short surface waves with wavelengths of a few centimeters. The SAR takes an instantaneous two-dimensional image of an area of about 100 km^2 . This large image maps the modulation of the short backscattering waves by the longer wind-driven waves. With reasonable assumptions the image can be inverted to obtain an estimate of the true two-dimensional wave number spectrum of the wind-driven waves.

An example of monthly mean significant wave heights from WAM compared with monthly mean H_s data from the TOPEX/POSEIDON altimeter and with H_s data retrieved from the SAR image spectra is presented in Figure 4. The monthly means for the year 1994 show quite a good agreement among the three different data sets. The latitudinal variation in the means of H_s is analogous to the variation in the mean wind speeds. The annual means of the H_s data in the northern extra-tropical, the tropical, and the southern extra-tropical latitudes amount to about 2.5, 2 and 3 m, respectively. As expected, the seasonal variation is larger in the northern

latitudes than in the southern latitudes and is negligibly small in the tropical latitudes. The slight overestimation evident in the modeled H_s data could later largely be remedied through revising the wave data analysis procedure. This comparison study provided promising results for the routine global wave modeling.

4.2 Synoptic-scale Wave Predictions

Synoptic wave predictions are conducted in real-time at several weather and wave prediction centers. Real-time predictions are beneficial for the routing of ships, the offshore industry and for safety services in coastal zones. This is particularly true for regions and times in which large deviations from the mean sea state can occur.

In the global ocean, the largest sea state variations occur in the northern storm track region. A typical example for large variations in the wind and wave data is shown by a 1993 time series taken from a location in the storm track of the Northeast Atlantic (Figure 5). The time series of the wave data are computed with the wave model WAM. The wave model was driven by analyzed winds of an atmospheric prediction model, which provided 6-hourly horizontal maps of wind vector fields. The local time series of wind and wave data, evidence a marked seasonal cycle: lower sea states during summer and higher sea states during winter. Overlaid on this seasonal cycle is the synoptic-scale variability on hourly to daily time scales. The synoptic wind variability includes an enhanced storm frequency during winter, and consequently in winter the wave heights are largest and the mean wave frequencies are lowest.

A more complete picture of the temporal evolution of wave properties is obtained from a time-sequence of two-dimensional wave spectra. As an example for a changing spectral energy distribution in response to a changing wind forcing, the situation occurring on January 10, 1993 in the northeastern Atlantic (Figure 5) is zoomed in. The wind strengthened from a moderate breeze of 5.7 ms^{-1} (corresponds to Beaufort 4) to a strong breeze of 13.6 ms^{-1} (Beaufort 6), and rotated from an eastward wind to a northwestward wind within 12 hours. The corresponding two-dimensional wave energy spectra computed with WAM are presented in Figure 6. Initially, the spectrum is composed of a wind sea partitioning propagating northeastward and a swell partitioning propagating southeastward. Twelve hours later, a new wind sea system has evolved through the northwestward directed wind forcing. The new wind sea system propagates in a northerly direction. The wind sea system shows a very broad angular spreading, because it is tied with the previous wind sea system through nonlinear interactions. The previous swell system still exists and reveals only little attenuation. Although the wind forcing and the spectral energy distribution changed considerably the mean wave characteristics are seen to change less abruptly with time. The total wave energy, expressed by significant wave height H_s , increased from 3.1 to 5 m, the mean frequency decreased slightly, while the mean wave propagation rotated anti-clockwise. This example clearly demonstrates, on the one hand, the relatively long lasting coexistence of wind sea and swell and, on the other hand, the relative large response time of a changing wind sea compared to an abrupt change in the wind forcing.

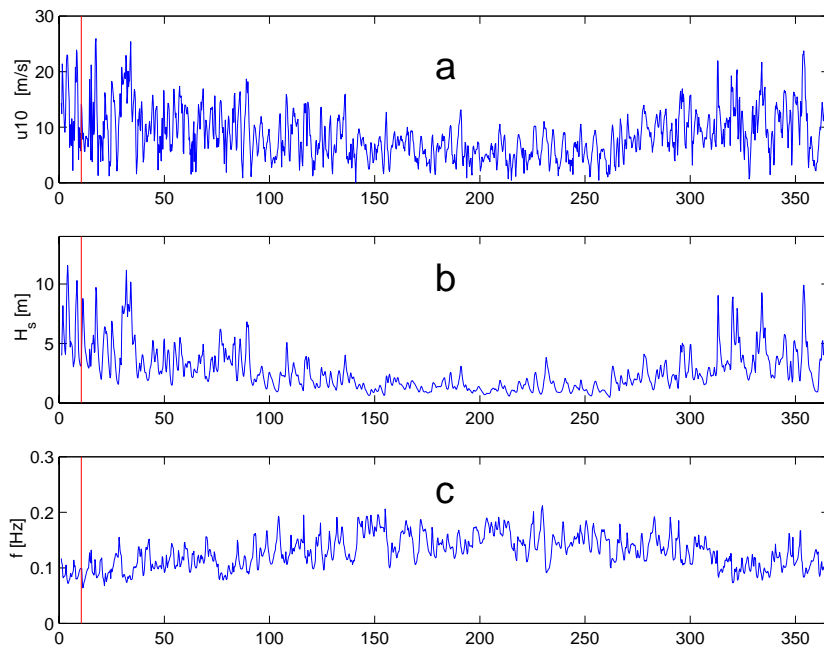


Figure 5: Wind speed u_{10} (m s^{-1}) in 10 m above ground from an atmospheric weather model (upper curve a), computed significant wave heights H_s in m (middle curve b) and mean wave frequency f in Hz (lower curve c) from a hindcast study with the wave model WAM. Time series are displayed for a location in the storm track of the Northeast Atlantic for the 365 days of 1993 with 6-hour resolution. The red line marks the rapid changes on January 10, 1993 from which the energy spectra are displayed in Figure 6.

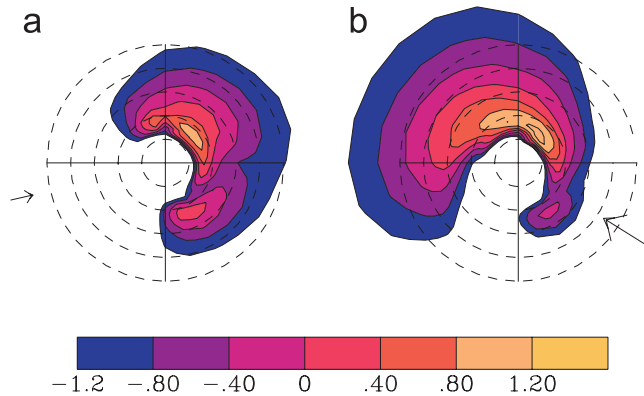


Figure 6: Polar diagram of wave energy spectra $E(f, \theta)$ (in logarithmic scaling) obtained from WAM for 2 instances 12 hours apart on January 10, 1993 showing the time evolution of wind sea and swell waves (compare Figure 5). The near-surface wind forcing in a) is 5.7 ms^{-1} into eastward direction and in b) 13.6 ms^{-1} into northwestward direction as indicated by arrows. The dashed circles indicate constant frequency which grows in steps of 0.05 Hz from the center to 0.025 Hz at the outer circle.

Comparisons of synoptic wave predictions with measurements suggest that further improvements are needed. The quality of wave predictions depends, in particular in regions with strongly varying winds, predominantly on the quality of the forcing wind fields. Therefore efforts on updating the real-time wave modeling are directed toward the combined analysis of winds and waves. A concept of a combined analysis procedure is sketched in Figure 7. The goal is to provide customers with real-time wave predictions of high quality. This can be pursued through the powerful technique of data assimilation.

4.3 Coupled Wind and Wave Data Assimilation

In general, data are assimilated into a physical system model to create an optimal analysis of model variables by merging the measured data with the dynamical model prediction. The accuracy of the dynamical model is known to be limited either through the coarse space-time resolution, or the approximate formulations describing the physical processes, or the uncertainties in the boundary values. A general presumption is that the measured data contain relevant information of the physical system with an accuracy larger than the accuracy of the model data. Thus through data assimilation model variables are updated which can then be utilized as initial conditions for forecast calculations. Forecast calculations with weather and wave prediction models cover usually several days.

First attempts at data assimilation were made in the first half of the 20th century to improve weather predictions by atmosphere models. Today, synoptic weather data are world-wide

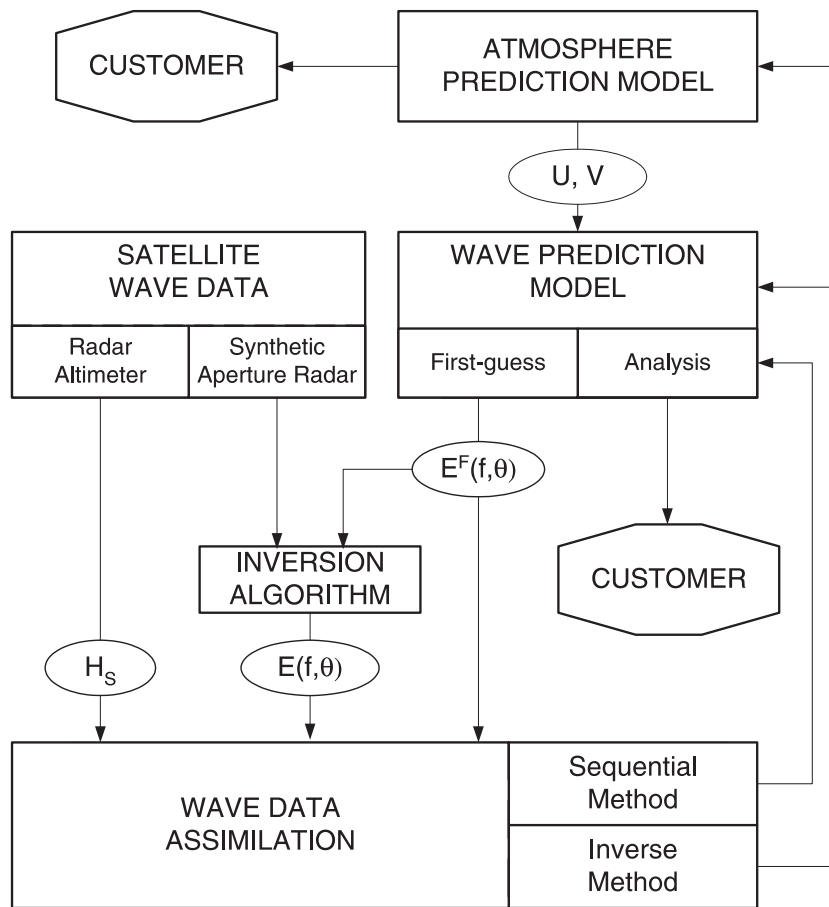


Figure 7: Concept of a combined wind and wave data assimilation scheme for real-time wave predictions. Central elements are the wave prediction model and the measured wave data by the radar altimeter and the Synthetic Aperture Radar (SAR) aboard polar orbiting satellites. Measured significant wave heights H_s and two-dimensional wave energy spectra $E(f, \theta)$ are merged with the first-guess model data $E^F(f, \theta)$ by the wave data assimilation scheme. The output are analyzed wave data available to customers. The combined wind and wave data assimilation scheme is evident from the fact that the wind corrections derived from the wave data assimilation are fed back to the atmosphere model. The thereby updated wind forcing (u, v) in turn produces a dynamical consistent update of the wave prediction.

recorded from ground stations and Earth observing satellites and are routinely exploited by data assimilation schemes in weather prediction centers. The initial operational data assimilation schemes used sequential techniques for assimilating the data from the synoptic network. A widely applied sequential technique is the Optimal Interpolation. During a time interval of typically 6 hours observed data are collected and then used to update the first-guess model data. The first-guess model data from the model prediction are updated by correction factors. These factors depend on the deviations between the model data and the measured data and on the error covariances of the data. Thus, analyzed model fields are produced every 6 hours for the subsequent prediction and the forecasts.

First attempts of assimilating wave data into a wave model were performed in the 1980s. Measured significant wave heights from the northern North Sea were assimilated into a wave model for the North Sea. In doing so, simple correction factors were applied to swell waves entering the North Sea, which improved the wave prediction in the southern North Sea. Thereafter, the Optimal Interpolation technique, seen to work successfully for weather predictions, was adopted for wave data assimilation. Eventually in August 1993, the assimilation of remotely sensed significant wave heights into the wave model WAM came in operation.

The sequential assimilation of H_s data from remote-sensing into the wave model WAM clearly revealed a positive impact on the wave forecast, however, the forecast skill was low. Three points for improvements became evident. First, ocean wave spectra are often not uni-modal, but are composed of different partitioning of wind sea and swell. Each partitioning has a different origin and therefore may contain different errors, calling for different corrections. Second, an update of a wind sea partitioning has to be accompanied by a consistent update of the local wind forcing. Otherwise the wave correction will rapidly be wiped out because the uncorrected winds will restore the erroneous wave spectrum. The large sensitivity of the waves to wind forcing indicates, that the assimilation of wave data also has the potential to correct wind errors. Third, the correction of the model wave energy has to be spread out in the region off incorrect wave energy propagation. Otherwise a localized wave correction will rapidly disappear through the continuing propagation of incorrect wave energy. For swell waves, this implies corrections backward along the propagation path to the location of the wave generation and also backward in the time.

The shortcomings in the sequential wave data assimilation method expedited the introduction of inverse methods, and the sparse information content of H_s data that of two-dimensional ocean wave spectra from satellite-based radar imaging. Measured two-dimensional spectra represent direct counterparts to the modeled spectra allowing the update of the partitioning of wind sea and swell differently. The most general inverse assimilation method is based on the adjoint model of the WAM model. The adjoint model of WAM was applied in research studies to refine the forcing and the dissipation function of the wave transport equation. Another specific inverse scheme, the so-called Green's function method, assimilates two-dimensional wave spectra and determines suitable wind corrections, which are then used to re-run the wave model to produce consistently corrected model wave spectra. The Green's function is based on a relation between small wind-wave changes, and is capable to compute wind corrections of young (present) and

old (past) wind forcing.

So far, experimental versions of inverse schemes for wave data assimilation have been tested. The results were promising; however, the methods are conceptually complex and computationally expensive. Therefore, further development is required, if they are going to be used in real-time wave prediction.

5 Outlook

In the second half of the 20th century considerable progress was made by cooperating scientific groups in developing a numerical prediction model for wind-driven surface waves. The concerted output was the third generation spectral wave model WAM, suitable for routine predictions of global wave energy spectra evolving from varying wind forcing. High-resolution, regional wave predictions are also practicable by modifying the specification of the model grid. Today, WAM is used by more than 40 wave modeling centers and research groups.

Spectral wave models are applied essentially in three different fields. First, global wave predictions are conducted to provide real-time information for ship routing, fisheries and offshore industries. Second, regional predictions of waves together with predictions of storm surges and tides are needed to guarantee the safety of humans and coastal constructions, and to prevent damage by the constant load of wave action as well as by extreme wave action. Third, analyses of long-term (decades and longer) simulations aim at estimating the wave climate and its potential modification due to global climate change.

The development of wave models is continued to consider regional effects of shallow water waves (SWAN, acronym for Simulated WAVes Nearshore) and higher-order numerical integration methods (WAVEWATCH III). Specifications of these spectral wave models may be found in the respective Internet sites. For regional wave modeling, alternatively to spectral wave modeling, also phase-resolving models are used. A phase-resolving model simulates amplitudes and phases of individual waves. The source functions in the wave propagation equation are included as simple amplification or decay factors. These models are applied, for instance, by engineers to compute wave-structure interactions needed for an optimal design of harbors.

The ongoing climate change is likely to considerably affect the global atmospheric circulation and thereby the wave climate. Changes in the wind fields, in particular in the frequency, duration, intensity and the path of storms, will in turn lead to changes in significant wave height, wave period and wave propagation direction. Given the central role that waves play in controlling the exchange of momentum, energy, gases, and aerosols at the sea surface, changes in the wave climate can be expected to feed back to physical and biophysical interaction processes in the atmosphere-ocean system. Studies of the potential feedback mechanisms commonly involve scenario simulations. It is tempting to claim that these simulations would gain in realism by taking into account climate-ocean wave interactions. Long term wave measurements have already provided first indications that the wave climate is changing in the second half of the 20th

century. However, data are still insufficient to draw solid conclusions on the mutual impact of global climate changes and wave climate changes.

Acknowledgments

The author is thankful to her colleagues Miguel A. Morales Maqueda, Antony Owinoh, and Ralf Weisse for their critical reading of the manuscript and their valuable comments. The author is also grateful to Gerbrant van Vledder for preparing Figure 3.

Annotated Bibliography

Apel J.R. (1987). *Principles of Ocean Physics*, 634 pp, Int. Geophysics Series, Vol. 38. [The book gives an concise overview of the essentials of modern physical oceanography including ocean wave physics. It also describes the acoustic, electromagnetic and optical aspects relevant for modern monitoring methods].

Boccotti P. (2000). *Wave mechanics for ocean engineering*, 495 pp, Elsevier Oceanographic Series, Vol. 64. [The book deals with a wide range of subjects related to the mechanics of waves and provides tools to estimates the wave loads on offshore structures].

Henderson F.M. and Lewis A.J. (1998). *Principles and applications of imaging radar, Manual of remote sensing*, 866 pp, John Wiley & Sons, Inc., Third Edition, Vol. 2. [This book contains a clear description of the fundamentals of radar imaging and presents numerous examples of applications in Geoscience].

Komen G.J., Cavaleri L., Donelan M., Hasselmann K., Hasselmann S. and Janssen P.A.E.M. (1994). *Dynamics and modelling of ocean waves*, 560 pp, Cambridge University Press, Cambridge (UK). [This book presents the fundamentals of wave theory in combination with wave measuring studies for validation of the forcing functions for the wave modeling. It also describes the current implementation of the third generation wave model WAM and different studies on wave data assimilation].

Massel S.R. (1996). *Ocean Surface Waves: Their Physics and Prediction*, 491 pp, Advanced Series on Ocean Engineering, Vol. 11, World Scientific, Singapore. [This book gives an elementary exposition of the mathematical and physical principles underlying the modern modeling methods for surface waves in deep and shallow water].

Massel S.R. (1999). *Fluid Mechanics for Marine Ecologists*, 566 pp Springer Verlag, Berlin. [This book presents in clear a manner the fundamentals of laminar and turbulent flow and the large-scale waves and currents and their link to aspects of marine ecology].

Monin A.S. (1990). *Theoretical Geophysical Fluid Dynamics*, 399 pp, Kluwer Academic Publishers, Dordrecht (NL). [The book provides a broad perspective of the theoretical description by using the Hamiltonian formalism and has special sections on processes as surface and internal waves and on global problems as the circulation of the atmosphere and the ocean].

Ochi M.K. (1998). *Ocean Waves, The stochastic approach*, 319 pp, Cambridge University Press, Cambridge Ocean Technology Series 6. [The book presents a broad overview of the

probability distributions of spectral wave data providing probabilistic predictions essential for the design of ships and structures exposed to the action of ocean waves].

The SWAMP Group (1985) *Ocean Wave Modeling*, 256 pp, Plenum Press, New York (USA). [This book describes the results of a systematic intercomparison study among nine different first and second generation wave models which led to the development of the third generation wave model].

Young I.R. (1999) *Wind Generated Ocean Waves*, 306 pp, Elsevier Ocean Engineering Book Series, Vol. 2, Elsevier Science. [The book is for engineers and scientists interested in the dynamics and kinematics of wind-generated waves with special emphasis on finite depth effects].

Internet sites

WAM: <http://www.dkrz.de/forschung/reports/report4/wamh-1.html>

SWAN: <http://swan.ct.tudelft.nl/>

WAVEWATCH III: <http://polar.wwb.noaa.gov/waves/wavewatch/wavewatch.html>

Inventory of European wave data base:
http://almeria.cedex.es/CEPYC/EU/inv_EWDB.html